RESEARCH ARTICLE SUMMARY

AMYLOIDOGENESIS

De novo design of a biologically active amyloid

Rodrigo Gallardo, Meine Ramakers, Frederik De Smet, Filip Claes, Ladan Khodaparast, Laleh Khodaparast, José R. Couceiro, Tobias Langenberg, Maxime Siemons, Sofie Nyström, Laurence J. Young, Romain F. Laine, Lydia Young, Enrico Radaelli, Iryna Benilova, Manoj Kumar, An Staes, Matyas Desager, Manu Beerens, Petra Vandervoort, Aernout Luttun, Kris Gevaert, Guy Bormans, Mieke Dewerchin, Johan Van Eldere, Peter Carmeliet, Greetje Vande Velde, Catherine Verfaillie, Clemens F. Kaminski, Bart De Strooper, Per Hammarström, K. Peter R. Nilsson, Louise Serpell, Joost Schymkowitz,* Frederic Rousseau*

INTRODUCTION: It has been shown that most proteins possess amyloidogenic segments. However, only about 30 human proteins are known to be involved in amyloid-associated pathologies, and it is still not clear what determines amyloid toxicity in these diseases. We investigated whether an endogenously expressed protein that contains sequences with known amyloidogenic segments, but is not known to aggregate either under normal or pathological conditions, can be induced to do so by seeding it with a peptide comprising the protein's own amyloidogenic fragment. We chose to target the protein vascular endothelial growth factor receptor 2 (VEGFR2) because it has well-characterized biological function and so could provide a model system with which to investigate the relationship between protein loss of function and amyloid toxicity in different cellular contexts.

RATIONALE: The capacity of the amyloid conformation of disease proteins to catalyze their own amyloid conversion demonstrates the sequence specificity of amyloid assembly. Because the core of amyloids consists of short amyloidogenic sequence fragments, we hypothesized that a short amyloidogenic protein sequence of VEGFR2, a protein normally not associated with protein aggregation, should be able to interact with and specifically induce the aggregation of VEGFR2, resulting in its functional knockdown. We used TANGO, an algorithm that predicts aggregation-prone sequences, to identify potential amyloidogenic fragments in VEGFR2. We synthesized these fragments as a tandem repeat in a peptide framework in which each unit is flanked by charged residues and coupled by a short peptide linker. The thinking behind this design was that the tandem repeats would promote the formation of diffusable soluble oligomeric aggregates, whereas the charged residues would kinetically stabilize these oligomers and reduce the rate of insoluble fibril formation.

RESULTS: By screening for loss of function, we identified one peptide, termed "vascin," that was highly potent at inhibiting VEGFR2. This sequence was derived from the translocation signaling sequence of VEGFR2. We found that vascin is an amyloidogenic peptide that readily forms small β-structured oligomers, ranging from dimers to nonamers, that slowly convert to amyloid fibrils. When added to cell culture medium, these oligomers are efficiently absorbed by the cell, where they interact with and promote the aggregation and partial degradation of nascent VEGFR2. Vascin aggregation does not induce the aggregation of known disease amyloids. Neither do vascin oligomers affect the function of the related EGF receptor or the surface translocation of other receptors. We found vascin only to be toxic to cells that are dependent on VEGFR2 function, suggesting that toxicity is due to loss of VEGFR2 function and not to vascin aggregation or vascin-induced VEGFR2 aggregation. Consistent with this, we found that vascin is active in vivo and could reduce tumor growth in a VEGFR2-sensitive subcutaneous B16 melanoma syngenic tumor model in mice but is not intrinsically toxic to other tissues.

CONCLUSION: We found that a short amyloidogenic protein fragment can induce the aggregation of a protein normally not associated with amyloidosis in a manner that recapitulates key biophysical and biochemical characteristics of natural amyloids. In addition, we found that amyloid toxicity is observed only in cells that both express VEGFR2 and are dependent on VEGFR2 activity for survival. Thus, rather than being generic, amyloid toxicity here appears to be both protein-specific and conditional on a requirement for VEGFR2 protein function. ■

ON OUR WEBSITE

Read the full article at http://dx.doi.org/10.1126/science.aah4949

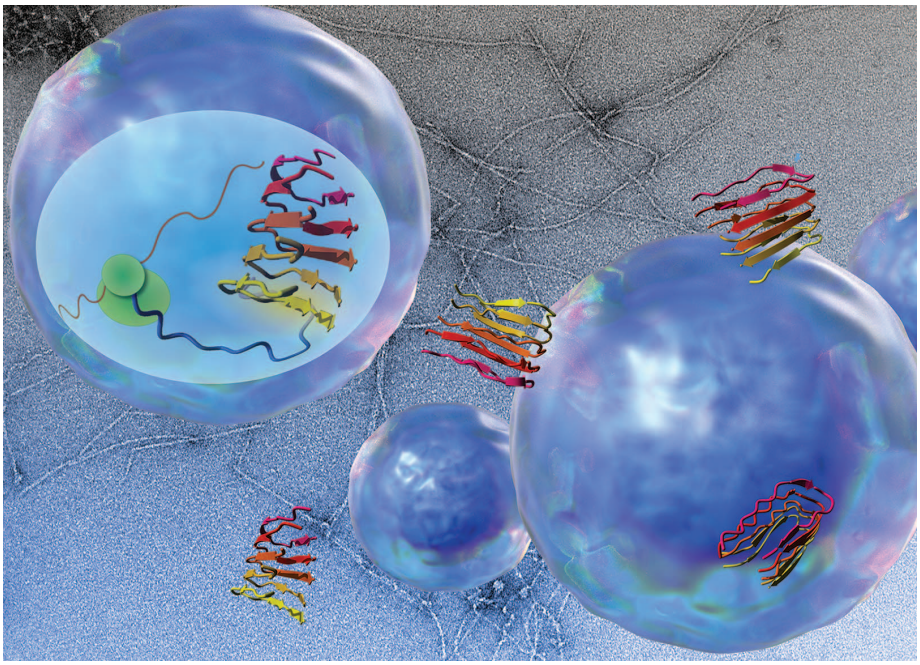

A synthetic amyloid peptide induces aggregation. We designed vascin, a synthetic amyloid peptide based on an amyloidogenic fragment of the signal peptide of VEGFR2. Vascin forms prefibrillar oligomers that penetrate mammalian cells and interacts with the nascent VEGFR2 protein, resulting in its aggregation and functional knockdown. [Composition includes parts of an image from iStock.com/luismmolina.]

The list of author affiliations is available in the full article online.
*Corresponding author. Email: frederic.rousseau@switch.vib-kuleuven.be (F.R.); joost.schymkowitz@switch.vib-kuleuven.be (J.S.)
Cite this article as R. Gallardo *et al.*, *Science* **354**, aah4949 (2016). DOI: 10.1126/science.aah4949

RESEARCH ARTICLE

AMYLOIDOGENESIS

De novo design of a biologically active amyloid

Rodrigo Gallardo,[1,2] Meine Ramakers,[1,2] Frederik De Smet,[1,2] Filip Claes,[1,2] Ladan Khodaparast,[1,2,3] Laleh Khodaparast,[1,2,3] José R. Couceiro,[1,2] Tobias Langenberg,[1,2] Maxime Siemons,[1,2,4] Sofie Nyström,[5] Laurence J. Young,[6] Romain F. Laine,[6] Lydia Young,[7,8] Enrico Radaelli,[9,10] Iryna Benilova,[9,10] Manoj Kumar,[11] An Staes,[12,13] Matyas Desager,[1,2,4] Manu Beerens,[14] Petra Vandervoort,[14] Aernout Luttun,[14] Kris Gevaert,[12,13] Guy Bormans,[4] Mieke Dewerchin,[15,16] Johan Van Eldere,[3] Peter Carmeliet,[15,16] Greetje Vande Velde,[17] Catherine Verfaillie,[11] Clemens F. Kaminski,[6] Bart De Strooper,[9,10] Per Hammarström,[5] K. Peter R. Nilsson,[5] Louise Serpell,[18] Joost Schymkowitz,[1,2]* Frederic Rousseau[1,2]*

Most human proteins possess amyloidogenic segments, but only about 30 are associated with amyloid-associated pathologies, and it remains unclear what determines amyloid toxicity. We designed vascin, a synthetic amyloid peptide, based on an amyloidogenic fragment of vascular endothelial growth factor receptor 2 (VEGFR2), a protein that is not associated to amyloidosis. Vascin recapitulates key biophysical and biochemical characteristics of natural amyloids, penetrates cells, and seeds the aggregation of VEGFR2 through direct interaction. We found that amyloid toxicity is observed only in cells that both express VEGFR2 and are dependent on VEGFR2 activity for survival. Thus, amyloid toxicity here appears to be both protein-specific and conditional—determined by VEGFR2 loss of function in a biological context in which target protein function is essential.

Amyloid aggregation of proteins is driven by short amyloidogenic sequence segments within a protein chain (*1*, *2*) that have the potential to self-assemble into β-sheet ribbons to form the characteristic cross-β–structured spine of amyloid structures (*3*, *4*). It has been shown that most proteins do in fact possess such amyloidogenic sequence segments (*5*, *6*). Still, only about 30 human proteins are known to be involved in amyloid-associated diseases (*7*, *8*). Moreover, it is still not clear what determines amyloid toxicity in these diseases (*8*, *9*). We investigated whether an endogenously expressed protein that possesses amyloidogenic potential but aggregates under neither normal nor pathological conditions can be induced to do so by seeding with a peptide consisting of an amyloidogenic fragment of its own sequence. The use of amyloidogenic fragment peptides is motivated by the observation that aggregation of disease-associated amyloidogenic proteins can be seeded by such peptides in vitro (*10*, *11*) and that truncations of amyloid proteins have been associated with increased seeding potential in vivo (*12*, *13*). Moreover, it has been shown that amyloidogenic peptides and proteins are generally much more efficient at seeding aggregation of homotypic sequences (*14*–*16*), although examples of cross-seeding do exist (*17*–*19*). Seeding of protein aggregation in vitro appears to work universally and fits with the structural model of aggregation as the addition of new strands to a growing amyloid fibril (*8*). This imparts sequence specificity to the seeding process because the incorporation of nonhomologous sequences into the highly ordered in-register stacking of identical side chains in the fibril core is likely to be energetically disfavored (*13*, *20*, *21*). The seeding concept appears to hold true both in cell culture and in vivo, even for non–prion aggregation–associated peptides and proteins, which have since been called "prionoids" (*22*). As a target protein, we chose vascular endothelial growth factor receptor 2 (VEGFR2) because the function of this protein is well characterized. To ensure efficient seeding, we designed an amyloidogenic peptide termed "vascin," which consists of a tandem repeat of an amyloidogenic sequence segment in the VEGFR2 signal peptide.

We found that vascin is a bona fide amyloidogenic peptide that forms mature cross-β fibrils along with prefibrillar intermediates, including soluble oligomers and protofibrils. Moreover, we found that the peptide is able to enter cells and reach the cytoplasmic compartment and specifically induce the aggregation of endogenous VEGFR2, inhibiting its function in human umbilical vein endothelial cells (HUVECs) in vitro and reducing VEGFR2-dependent tumor progression in vivo.

It remains unclear what determines amyloid toxicity in amyloid diseases and whether cell death results from a consequence of direct amyloid toxicity (gain of function) or whether it is a consequence of loss of function (*23*, *24*). However, our detailed understanding of real amyloid disease models is often insufficient to address these questions directly. For many disease-associated amyloidogenic proteins—such as the β-amyloid (Aβ) peptide in Alzheimer's disease (*25*) and α-synuclein in Parkinson's disease (*26*)—we still have insufficient understanding both of their physiological role as well as the cellular interactions of the amyloid conformation in disease (*26*, *27*). We do, however, have a better understanding of the structural and biochemical characteristics that are common to most amyloid diseases. These features include the cross-β structural organization of the spine of the amyloid fibrils formed by short segments of the sequence; the population of prefibrillar intermediates, including soluble oligomers and protofibrils; and the capacity of amyloids to seed aggregation of the native conformation. Although our artificial amyloid model recapitulates these key structural and biochemical features of natural amyloids, it is also simple enough to investigate the relationship between protein loss of function and amyloid toxicity.

Our results show that vascin amyloids are not inherently toxic but that the emergence of amyloid toxicity is dependent on biological context. Vascin is not toxic to cells that do not express VEGFR2 or to cells expressing VEGFR2 but that are not dependent on VEGFR2 function. However, when introduced in VEGFR2-dependent cells, we found association of vascin amyloid toxicity and VEGFR2 loss of function. Therefore, our model system demonstrates that amyloidogenic protein fragments can induce aggregation of nonamyloidogenic proteins and that under these conditions, amyloid

[1]VIB Switch Laboratory, Leuven, Belgium. [2]Department for Cellular and Molecular Medicine, Katholieke Universiteit Leuven (KU Leuven), Belgium. [3]Laboratory of Clinical Bacteriology and Mycology, Department of Microbiology and Immunology, KU Leuven, Belgium. [4]Laboratory of Radiopharmacy, Department of Pharmaceutical and Pharmacological Sciences, KU Leuven, Belgium. [5]IFM Department of Chemistry, Linköping University, Linköping, Sweden. [6]Department of Chemical Engineering and Biotechnology, University of Cambridge, New Museums Site, Pembroke Street, Cambridge CB2 3RA, UK. [7]Astbury Centre for Structural Molecular Biology, University of Leeds, Leeds, UK. [8]School of Molecular and Cellular Biology, University of Leeds, Leeds, UK. [9]VIB Center for the Biology of Disease, 3000 Leuven, Belgium. [10]Center for Human Genetics and Leuven Institute for Neurodegenerative Diseases (LIND), KU Leuven, 3000 Leuven, Belgium. [11]Stem Cell Institute, KU Leuven, Leuven, Belgium. [12]VIB Medical Biotechnology Center, VIB, Ghent, Belgium. [13]Department of Biochemistry, Ghent University, Ghent, Belgium. [14]Department of Cardiovascular Sciences, Center for Molecular and Vascular Biology Research Unit, Endothelial Cell Biology Unit, KU Leuven, B-3000 Leuven, Belgium. [15]Laboratory of Angiogenesis and Vascular Metabolism, Department of Oncology, KU Leuven, B-3000 Leuven, Belgium. [16]Laboratory of Angiogenesis and Vascular Metabolism, Vesalius Research Center, VIB, Leuven B-3000, Belgium. [17]Biomedical MRI Unit/MoSAIC, Department of Imaging and Pathology, KU Leuven, Leuven, Belgium. [18]School of Life Sciences, University of Sussex, Falmer, East Sussex BN1 9QG, UK.
***Corresponding author. Email: frederic.rousseau@switch.vib-kuleuven.be (F.R.); joost.schymkowitz@switch.vib-kuleuven.be (J.S.)**

gain of function is a phenotypic effect resulting from cell-context–specific loss of function.

Results

Design of vascin, an amyloidogenic peptide derived from a VEGFR2 fragment

We analyzed the VEGFR2 proteins from mouse and human using the statistical thermodynamics algorithm TANGO (fig. S1A) (28). Because we envisaged testing the sequence ultimately in a mouse model, we opted for maximal compatibility with the mouse protein. Moreover, the two homologs share 84% sequence identity overall and 90% in the TANGO regions. To derive peptide sequences that are likely to form amyloid structure in isolation, but also have a high potential for forming soluble oligomers (29), we devised a strategy (30, 31) that makes use of a sequence feature of functional amyloids and yeast prions, which often contain several aggregation-prone regions (APRs) (32) closely connected by disordered regions (33). Hence, we placed two APRs in a peptide, separated by a rigid proline-proline linker, mimicking these repeat patterns. In order to maintain colloidal stability and solubility of the sequence, we supercharged the peptides by flanking the APRs with either negatively charged aspartate or positively charged arginine residues. Given the length limitations imposed by the efficiency of solid-phase peptide synthesis, this design scheme imposes a length limitation on the APRs of seven amino acids. Hence, we selected 10 such high-scoring sequences (table S1) and generated the 38 peptide sequences listed in table S2, which explore both tandem repeats of the same APR as well as fusions of different APRs. Peptides were screened for their ability to inhibit VEGF signaling in human embryonic kidney (HEK) 293 cells transfected with mouse VEGFR2. To this end, cells were treated overnight with an apparent concentration of 20 μM peptide (assuming 100% synthesis efficiency), and extracellular signal–regulated kinase (ERK) phosphorylation was determined after stimulation for 5 min with 25 ng/mL VEGF (fig. S1B). At this concentration, we observed inhibition only with two peptides (B8 and B12). The effect was most pronounced with the peptide B8, which was based on a tandem repeat of the first high-scoring aggregation-prone region in the sequence that belongs to the signal peptide and has the sequence $L_6AVALWF_{12}$ (fig. S2A), resulting in the sequence DLAVALWFDPPDLAVALWFD [isoelectric point (pI) = 3.38, molecular weight (MW) = 2272.15 Da]. We termed this peptide vascin (fig. S2B), obtained additional material by means of solid-phase peptide synthesis followed by high-performance liquid chromatography purification (fig. S2C), and confirmed its identity with mass spectrometry (observed mass, 2272.4) (fig. S2D).

Vascin forms soluble β-structured oligomers that mature into amyloid fibrils

To determine the amyloidogenic nature of the peptide, vascin was dissolved to a final concentration of 300 μM in 1% (w/v) ammonium bicarbonate in ddH_2O. After 24 hours of incubation, transmission electron microscopy (TEM) revealed typical amyloid fibrils of ~10 nm in width consisting of protofilaments of 4 to 5 nm (Fig. 1, A to D, and fig. S3). Additionally, vascin fibrils bind amyloid sensor dyes, including thioflavin-T and the amyloid-specific oligothiophene h-HTAA (Fig. 1E) (34). X-ray diffraction of aligned bundles of vascin fibrils confirmed their cross-β nature, with characteristic diffractions at 4.7 and 10 Å (Fig. 1F). Together, these data confirm the amyloidogenic nature of vascin. In order to follow amyloid formation kinetics, we filtered 100 μM dissolved vascin 1% (w/v) ammonium bicarbonate in ddH_2O through a 0.2-μm regenerated cellulose filter and monitored particle size distribution using electrospray ionization–mass spectrometry linked to ion mobility spectrometry (ESI-IMS-MS) (Fig. 1G) (35) and dynamic light scattering (DLS) (Fig. 1H). At time zero, the MS resolved a mixture of monomers and multimers up to heptamers (Fig. 1G), whereas the particle sizes estimated through DLS ranged from 5 to 100 nm (assuming linear polymer particles). This indicates that the filtered vascin solution contains soluble oligomeric aggregates already at time zero. After 6 hours, particles reached sizes over 1 μm (Fig. 1H). The fact that no lag phase was observed in the evolution of the DLS autocorrelation function (fig. S4, A and B) further suggests that these soluble oligomers are able to directly proceed to amyloid fibril formation. In order to probe the secondary structure of these soluble aggregates, we monitored the same aggregation kinetics using Fourier transform infrared (FTIR) spectroscopy. The spectrum at time zero was dominated by maxima near 1630 and 1690 cm^{-1} (Fig. 1I), which is characteristic of β-sheet structure. Over the following 3 hours, the intensity of these peaks increased markedly, whereas the center of the peaks shifted gradually to 1622 and 1692 cm^{-1}, respectively (Fig. 1, I and J). These peaks were quite narrow, and regions outside the peaks showed very little absorption, suggesting that most of the peptide sequence is involved in β-structured hydrogen bonding. FTIR kinetics therefore indicate that vascin largely adopts a β-structured conformation upon solubilization in 1% ammonium bicarbonate and that these species mature into amyloid fibrils over time. Last, we measured binding to 8-anilino-1-naphthalenesulphonic acid (ANS) during vascin amyloid formation (fig. S4C), revealing high binding of this dye at time zero. The latter is a typical feature of interaction-prone cytotoxic prefibrillar oligomers that present a high degree of solvent-exposed hydrophobic surface (36). The binding of ANS increased over time, suggesting that hydrophobic surfaces stay exposed upon fibril formation. We also verified the amyloidotypic double peak fluorescence spectrum of vascin with the luminescent conjugated oligothiophene hHTAA in contrast to the scrambled peptide (fig. S4D). Given that the above observations were made at 300 μM peptide, in which the signal-to-noise ratio for biophysical characterization is optimal, we also verified that vascin readily formed amyloid fibrils at the lower concentration of 30 μM (fig. S5). Compared with vascin, a scrambled version of the peptide (supplementary text, note S1) formed small soluble aggregates with hydrodynamic radii smaller than 100 nm, as estimated by means of DLS (fig. S6 A and B), that exhibited a nonfibrillar morphology via TEM (fig. S6C) and displayed marginal affinity for the amyloid sensor dyes, with no specific emission spectrum for amyloid fibers (Fig. 1E and fig. S4D). Similar observations were made with a vascin variant in which proline mutations were introduced to break the β-sheet propensity of the APRs in vascin (supplementary text, note S2, and fig. S7). In contrast, a version of vascin based on the human sequence (h. vascin, DLAVALWLDPPDLAVALWLD), containing a single mutation of phenylalanine to leucine at position 7 of the APR, displayed similar amyloid formation as that of the original mouse sequence (fig. S8).

The biophysical characterization above confirms that vascin is an amyloidogenic peptide that readily forms β-structured soluble oligomeric aggregates that mature into cross-β–structured amyloid fibrils in a broad concentration range.

Vascin inactivates VEGFR2 in HUVECs by specifically inducing its aggregation

Because vascin is an amyloidogenic peptide derived from a VEGFR2 fragment, we investigated whether it displays biological activity toward VEGFR2 in cultured cells. First, we monitored cellular uptake of vascin using carboxyfluorescein-labeled vascin (CF-vascin) in HUVECs. We observed cellular uptake during the first hour of incubation as small vesicles or inclusions that contained diffuse homogeneous peptide (Fig. 2A). Moreover, these inclusions were positive for the amyloid sensor dye pFTAA (Fig. 2, B and C), showing that the peptide remains in an amyloid-like conformation inside the cells. Co-staining for the endoplasmic reticulum (ER) protein calnexin revealed that the peptides are on the cytoplasmic side of the ER (Fig. 2D), where they partially overlap with staining for ribosomes (Fig. 2E). Proximity ligation (Duo-Link) by using antibodies against VEGFR2 and the carboxyfluorescein label on vascin (Fig. 2F), quantified by use of image analysis from high-content microscopy, demonstrated direct interaction between vascin and VEGFR2 (Fig. 2G). This result was further confirmed with two-color direct stochastic optical reconstruction microscopy (*d*STORM) super-resolution imaging (37) by using 0.5 μM of Alexa647-labeled vascin and Alexa568-labeled immunodetection of VEGFR2 (Fig. 2, H and I).

Coimmunoprecipitation of VEGFR2 from lysates of vascin-treated HUVECs was performed with polyethylene glycol (PEG)–biotin–labeled peptide, again demonstrating direct interaction between vascin and VEGFR2 (Fig. 3A). To investigate the consequences of the interaction between vascin and VEGFR2 on the aggregation status of the receptor, we determined the difference in distribution of VEGFR2 between soluble and insoluble fractions of lysates from HUVECs treated with 20 μM vascin. Upon vascin treatment, we could observe a clear redistribution of full-length and partially degraded VEGFR2 toward the insoluble

fraction, whereas this was not the case upon treatment with scrambled vascin (Fig. 3B). In addition, the induced insoluble VEGFR2 displays partial resistance to the ionic detergent SDS, a hallmark of amyloid-like aggregation (Fig. 3C). To confirm that vascin-mediated aggregation of VEGFR2 in HUVECs leads to its loss of function, we determined the dose-response curve of vascin on VEGFR2 autophosphorylation and ERK phosphorylation [mesoscale discovery enzyme-linked immunosorbent assay (MSD ELISA)] after stimulating HUVECs for 5 min with 1.3 nM VEGF. HUVECs displayed a clear dose-responsive inhibition by vascin with a median inhibitory concentration (IC_{50}) of 6.8 ± 0.5 μM for receptor autophosphorylation and 8.3 ± 0.4 μM for ERK phosphorylation (Fig. 3, D and E). The human version of vascin showed similar inhibition, which was not observed when using the scrambled or proline controls (Fig. 3F). Using fluorescence-activated cell sorting (FACS), we observed a concomitant reduction in the surface expression of VEGFR2 in HUVECs, but not of the unrelated cell-surface protein CD29 (Fig. 3G and fig. S9), confirming loss of VEGFR2 function in HUVECs. Together, these data show that vascin is internalized by HUVECs and reaches the cytoplasmic compartment, where it directly binds to VEGFR2 and localizes with ribosomes, resulting in the functional inactivation through aggregation of VEGFR2. This effect seemed to be specific, as

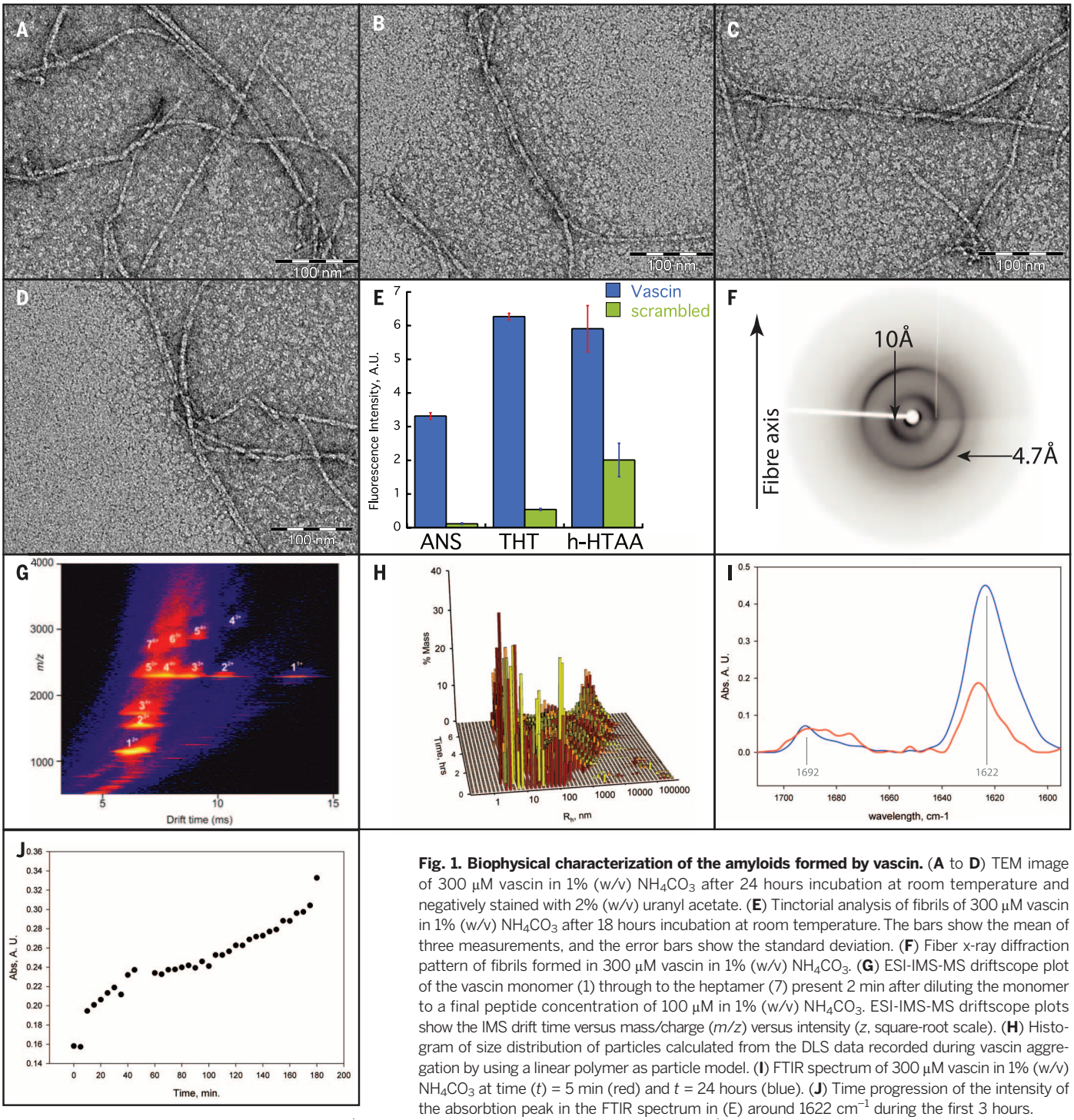

Fig. 1. Biophysical characterization of the amyloids formed by vascin. (**A** to **D**) TEM image of 300 μM vascin in 1% (w/v) NH_4CO_3 after 24 hours incubation at room temperature and negatively stained with 2% (w/v) uranyl acetate. (**E**) Tinctorial analysis of fibrils of 300 μM vascin in 1% (w/v) NH_4CO_3 after 18 hours incubation at room temperature. The bars show the mean of three measurements, and the error bars show the standard deviation. (**F**) Fiber x-ray diffraction pattern of fibrils formed in 300 μM vascin in 1% (w/v) NH_4CO_3. (**G**) ESI-IMS-MS driftscope plot of the vascin monomer (1) through to the heptamer (7) present 2 min after diluting the monomer to a final peptide concentration of 100 μM in 1% (w/v) NH_4CO_3. ESI-IMS-MS driftscope plots show the IMS drift time versus mass/charge (*m/z*) versus intensity (*z*, square-root scale). (**H**) Histogram of size distribution of particles calculated from the DLS data recorded during vascin aggregation by using a linear polymer as particle model. (**I**) FTIR spectrum of 300 μM vascin in 1% (w/v) NH_4CO_3 at time (*t*) = 5 min (red) and *t* = 24 hours (blue). (**J**) Time progression of the intensity of the absorbtion peak in the FTIR spectrum in (E) around 1622 cm^{-1} during the first 3 hours.

indicated by the CD29 result. Moreover, we observed no effect of vascin on EGF signaling in HeLa cells, which do not endogenously express VEGFR2 but the functionally homologous EGFR. Treatment of this cell line with 20 μM vascin showed no inhibition of ERK phosphorylation when stimulated with EGF (Fig. 3H), showing that the inhibitory effect of vascin on ERK phosphorylation is specific for VEGFR2 stimulation. To test whether known amyloidogenic proteins were affected by vascin, we investigated the effect of adding vascin to solutions of the Alzheimer β-peptide 1-42 (Aβ) (Fig. 3I) or the human prion protein (PrP) (Fig. 3J) and monitored aggregation through ThT fluorescence emission. The mean lag time for unseeded aggregation of Aβ1-40 was 350 min, whereas addition of preformed Aβ fibrils decreased the lag time to 130 min. Addition of vascin fibril variants did not lead to significant decrease of fibrillation lag times other than for scrambled vascin, where the significance level in a paired t test was $P > 0.03$. The mean lag time for spontaneous conversion of HuPrP23-231 was 1100 min. The conversion rate upon addition of preformed HuPrP90-231 fibrils was shortened to 135 min, whereas addition of preformed vascin fibril variants did not lead to significant alteration of lag time. These data demonstrate that no vascin cross-seeding occurs for these proteins.

Vascin reduces VEGFR2-dependent tumor growth in mice

To establish the effect of vascin in vivo, we turned to a functional angiogenesis model that is sensitive to inhibition of VEGFR2 in vivo and used a subcutaneous B16 melanoma syngenic tumor model in C57BL/6 inbred mice. Tumor growth of this line is strongly reduced by VEGFR2-specific inhibition approaches, such as the tyrosine kinase inhibitor protein tyrosine kinase (PTK) 787/ZK 222584 (38), providing a sensitive phenotypic

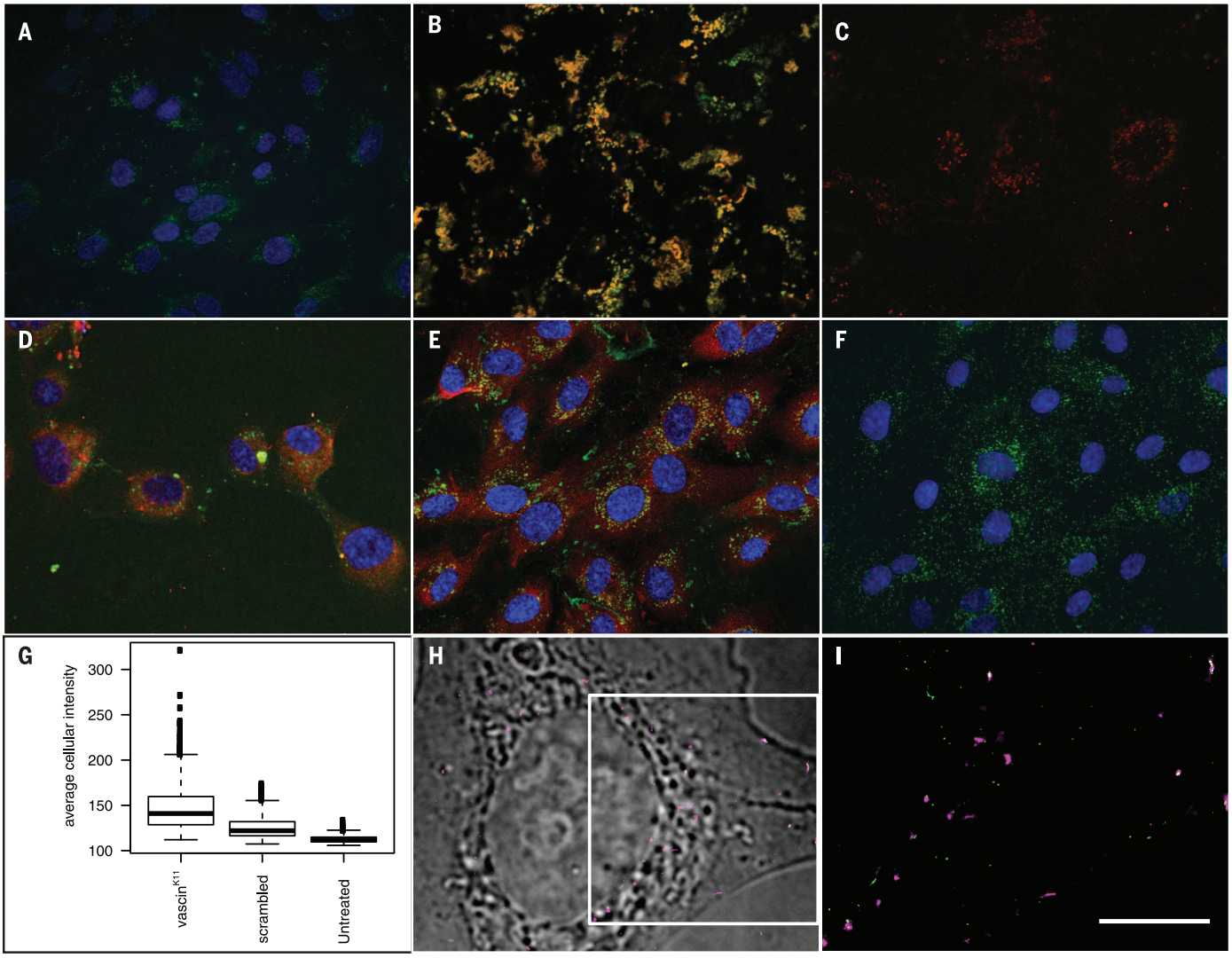

Fig. 2. Vascin directly interacts with VEGFR2 in cells. (**A**) Cellular distribution of CF-vascin^{K11} (green) at 1 μM in HUVECs. (**B**) Overlay between the fluorescence of Alexa647-labeled vascin^{K11} (20 μM, red) and the amyloid-specific dye pFTAA (15 μM, green). Overlap is shown as yellow coloring. (**C**) Equivalent image as (B) for the proline mutant of vascin. (**D**) HUVECs treated for 4 hours with CF-vascin^{K11} (2.5 μM, green) and co-immunostained for the ER-specific marker calnexin (red). (**E**) HUVECs treated for 4 hours with CF-vascin^{K11} (5.0 μM, green) and co-immunostained for the ribosomal protein S6 (red). (**F**) Proximity ligation (Duo-Link) between CF-vascin^{K11} at 5.0 μM and VEGFR2 performed in HUVECs treated for 4 hours with peptide. For (A), (D), (E), and (F), the nuclei are stained with 4′,6-diamidino-2-phenylindole in blue. (**G**) Quantification of the Duo-Link signal by high-content microscopy of HUVECs treated with vascin as depicted in (E). For each condition, ~700 cells were analyzed, and the average fluorescence intensity per cell is shown. The box shows the interquartile range of the 25 to 75 percentile. The line in the middle of the box indicates the median, and the lines extending from the box indicate the 99% limits of the distribution. Outliers are shown as squares. (**H**) dSTORM image of HUVECs treated for 4 hours with 0.5 μM Alexa647-labeled vascin^{K11} (purple) and co-immunostained for VEGFR2 (green). Scale bar, 1 μm. (**I**) Magnification of image in (G). White pixels indicate the interaction of vascin and VEGFR2. Scale bar, 1 μm.

readout for the anticipated effect of vascin. To assess whether vascin administration would be tolerated by C57BL/6 mice, we first performed a dose-escalation study by means of daily intravenous tail vein injection in two 6-week-old, inbred C57BL/6 mice, starting from 1 to 10 mg/kg PEG-biotin vascin, which corresponded to the highest stock concentration of the peptide that we could reach with the available material. No adverse effects to

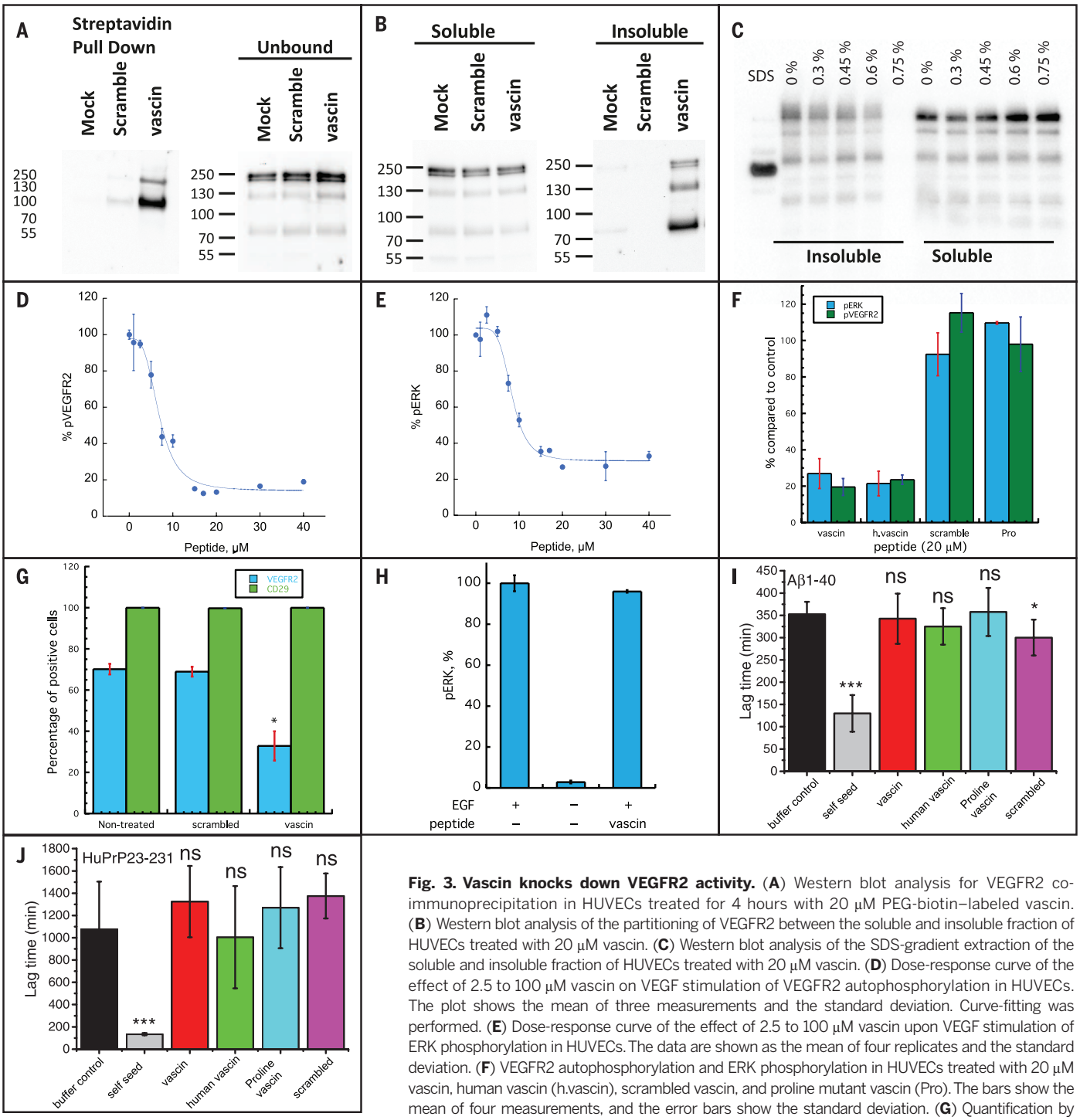

Fig. 3. Vascin knocks down VEGFR2 activity. (**A**) Western blot analysis for VEGFR2 co-immunoprecipitation in HUVECs treated for 4 hours with 20 μM PEG-biotin–labeled vascin. (**B**) Western blot analysis of the partitioning of VEGFR2 between the soluble and insoluble fraction of HUVECs treated with 20 μM vascin. (**C**) Western blot analysis of the SDS-gradient extraction of the soluble and insoluble fraction of HUVECs treated with 20 μM vascin. (**D**) Dose-response curve of the effect of 2.5 to 100 μM vascin on VEGF stimulation of VEGFR2 autophosphorylation in HUVECs. The plot shows the mean of three measurements and the standard deviation. Curve-fitting was performed. (**E**) Dose-response curve of the effect of 2.5 to 100 μM vascin upon VEGF stimulation of ERK phosphorylation in HUVECs. The data are shown as the mean of four replicates and the standard deviation. (**F**) VEGFR2 autophosphorylation and ERK phosphorylation in HUVECs treated with 20 μM vascin, human vascin (h.vascin), scrambled vascin, and proline mutant vascin (Pro). The bars show the mean of four measurements, and the error bars show the standard deviation. (**G**) Quantification by means of FACS of the fraction of cells that display VEGFR2 and CD29 on the cell surface upon treatment with vascin or scrambled vascin at 20 μM. Per condition, 10,000 cells were analyzed. The bars show the mean of three measurements, and the error bars show the standard deviation. *$P < 0.05$ calculated by Student's t test compared with the nontreated condition. (**H**) Quantification of ERK phosphorylation level as determined by means of MSD assay upon EGF stimulation of HeLa cells treated with 20 μM vascin. The data are shown as the mean of four replicates and the standard deviation. (**I**) Lag phase of the aggregation kinetics of the Alzheimer β-peptide 1-40 (Aβ1-40) observed with Thioflavin T fluorescence in the presence of 1% molar fraction of homotypic seeds (self seed), or the equivalent amount of seeds of vascin, human vascin, scrambled vascin, or the proline mutant vascin. (**J**) Equivalent experiment to (I) for the human prion protein (HuPrP23-231). All aggregation kinetics experiments were run in six replicates, and the bars show the mean value, with error bars showing the standard deviation. The statistically significant differences were identified using the Student's t test.

the basic physiological and behavioral parameters of the animals were apparent across this concentration range, including body weight, food and water consumption, home cage activity, and locomotion. To test the effect of vascin on tumor growth, B16 cells were injected subcutaneously in the right dorsal flank of 8-week-old C57BL/6 mice. Starting from 3 days after tumor injection and until day 17, mice were treated daily by means of intravenous injection of 10 mg/kg PEG-biotin vascin (n = 10 mice) or scrambled vascin as the negative control (n = 10 mice). Another negative control group received intravenous injection of the vehicle (50 mM Tris HCl pH 7.5, n = 10 mice), and the positive control group (n = 5 mice) received the kinase inhibitor PTK787 orally (75mg/kg). Tumor growth was similar in animals treated with scrambled vascin or vehicle and markedly reduced in animals that received the PTK inhibitor. In the vascin-treated group, tumor growth was significantly inhibited compared with that in the negative controls over the entire experiment [analysis of variance (ANOVA) with Tukey post-hoc] and up to day 14 to a similar extent as the PTK-treated group (Fig. 4A).

In order to exclude overall toxicity effects of vascin on the general physiology of the mouse, we executed a short-term toxicology study in which we treated groups of five mice daily with intravenous injections of vascin (10 mg/kg, group A), scrambled (10 mg/kg, group B), or vehicle (50 mM Tris pH 7.5) for 14 days (the same duration as that of the tumor growth experiment). Gross examination at necropsy did not reveal any macroscopic changes (fig. S10A). Concerning organ weights (fig. S10B), hematology (fig. S10C), and clinical chemistry (fig. S10D), no statistically significant differences were observed among groups. Also, no significant variations were observed among the experimental groups in terms of lesion spectrum, frequency, and severity. In addition, we examined brain sections from all the animals for amyloid deposition and associated astrogliosis. Thioflavin-S–positive deposits in the brain parenchyma were not detected (fig. S11, A, B, and C), and co-staining with GFAP (glial fibrillary acidic protein) did not show any morphological evidence of astrogliosis, in sharp contrast to the positive control (fig. S11D), for which we used a transgenic Alzheimer's disease mouse model that has marked amyloid deposition throughout the cortex and hippocampus (*39*).

In order to demonstrate the arrival and presence of vascin at the tumor site, two groups of tumor-bearing mice were injected intravenously with 10 mg/kg CF-vascin or vehicle (50 mM Tris HCl pH 7.5, negative control) and imaged with whole-body fluorescence imaging. Because the melanin expression by the tumors strongly absorbs light, which hampers the in vivo detection of

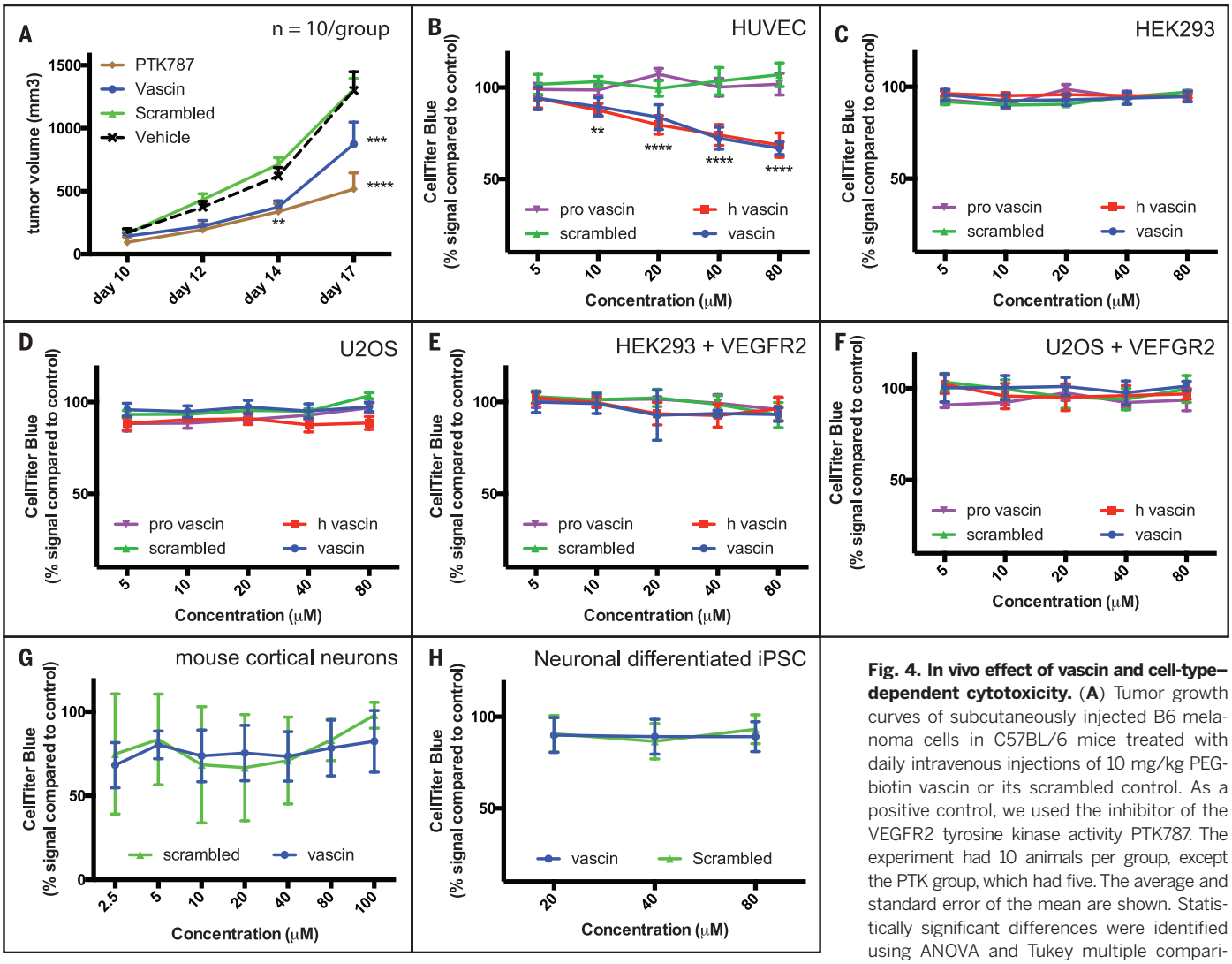

Fig. 4. In vivo effect of vascin and cell-type–dependent cytotoxicity. (**A**) Tumor growth curves of subcutaneously injected B6 melanoma cells in C57BL/6 mice treated with daily intravenous injections of 10 mg/kg PEG-biotin vascin or its scrambled control. As a positive control, we used the inhibitor of the VEGFR2 tyrosine kinase activity PTK787. The experiment had 10 animals per group, except the PTK group, which had five. The average and standard error of the mean are shown. Statistically significant differences were identified using ANOVA and Tukey multiple comparison testing. (**B** to **H**) Dose-dependent toxicity of vascin or its scrambled control tested from 2.5 to 100 μM by the CellTiter-Blue assay on (B) HUVECs, (C) HEK293 cells, (D) U2OS cells, (E) HEK293 cells transiently overexpressing VEGFR2, (F) U2OS cells transiently overexpressing VEGFR2, (G) cortical primary neuron cells from mouse, and (H) cortical neuronal progeny obtained from human iPSCs after a neuronal differentiation protocol. All toxicity data are shown as the mean of five measurements with standard deviations, except the iPSC data, which were 48 replicates. Statistically significant differences were identified by using ANOVA and Tukey multiple comparison testing.

fluorescence, tumors were isolated 30 min after injection and imaged ex vivo. The resulting fluorescence images showed strong green fluorescence emission for tumors isolated from CF-vascin–injected mice, whereas no fluorescence could be detected from tumors isolated from vehicle-injected control mice (fig. S12A), supporting the presence of vascin-CF at the tumor site according to macroscopic CF-fluorescence measurements. To further verify the presence of CF-vascin inside the tumor tissue with microscopic resolution, we additionally examined the presence of CF-vascin with fibered confocal fluorescence microscopy (FCFM) on tumor samples from the same mice. Inserting the fiber-optical probe inside the tumor tissue sample of vehicle-injected control mice did not show any fluorescence signal, whereas the tumor samples of CF-vascin–injected mice were clearly positive for green fluorescence (fig. S12B). To quantify vascin in B16 tumors, the specific light absorption by melanomas was calibrated through the addition of different known quantities of CF-vascin to series of tumor tissue dilutions and compared with a standard curve of fluorescence intensity for a dilution series of pure CF-vascin. Both were found to be linear in a large concentration range and for two different fluorescence imaging modalities, cross-validating the results (fig. S13, A and B). The tumor-specific fluorescence attenuation was then used to estimate the concentration of CF-vascin in tumors isolated from CF-vascin–treated mice, which was established to be 26.4 ± 10.5 μM, a concentration that is well above the IC_{50}.

Taken together, these data are consistent with a direct inhibitory activity of vascin on VEGFR2 function in vivo in the same manner that was observed in cells.

Amyloid toxicity is conditional to VEGFR2 dependence of cells

We determined loss of VEGFR2 function and vascin amyloid toxicity in several cell lines. CellTiter-Blue cytotoxicity assays (Fig. 4B) revealed that in HUVECs, loss of function of the receptor (IC_{50} of 6.8 ± 0.5 μM for receptor autophosphorylation and 8.3 ± 0.4 μM for ERK phosphorylation) goes hand in hand with cytotoxicity. On the other hand, in HEK293 or U2OS cells neither 2.5 to 100 μM of vascin nor its scrambled counterpart were found to be toxic (Fig. 4, C and D). Upon transfection of VEGFR2 in HEK293, we observed that after VEGF stimulation, ERK phosphorylation was inhibited upon treatment with 20 μM vascin (fig. S14A), which induced the aggregation of the VEGFR2, as evidenced on the fractionation assay (fig. S14B). However, no noticeable toxicity of vascin to HEK293 cells expressing VEGFR2 was observed in the range of 2.5 to 100 μM (Fig. 4E). This demonstrates that vascin is not toxic to HEK293 cells in the absence of VEGFR2 but also that aggregation of transiently expressed VEGFR2 in these lines does not affect cell viability. Similar observations were made with U2OS cells expressing VEGFR2 (Fig. 4F). Thus, vascin does not display generic amyloid toxicity, and the aggregation of VEGFR2 by vascin is in itself also not toxic. Last, because neurons are particularly sensitive to aggregate toxicity, we assessed the toxicity of vascin to primary cortical neurons, which do not express VEGFR2. Although with these neurons we observed significant toxicity upon peptide treatment (Fig. 4G), CellTiter-Blue reaction levels were similar for the vascin and its scrambled non-amyloid variant, suggesting that the toxicity was not amyloid-specific but rather reflects the high sensitivity of these cultures, which also resulted in a large variability in the assay. To verify this further, we turned to human induced pluripotent stem cells (iPSCs) differentiated to a cortical neuronal phenotype, which was verified by using quantitative reverse transcription polymerase chain reaction and immunostaining for markers specific for this cell type (fig. S15). In these cultures, we observed a lack of amyloid-specific toxicity, although there is 10% toxicity associated with administration of vascin or the scrambled control (Fig. 4H).

Together, these data suggest that amyloid toxicity is not dependent on cell type or even on target protein aggregation, but that amyloid toxicity is mainly determined from the biological context in which the target protein is inactivated by aggregation. Because HUVEC survival is dependent on VEFGR2 function, its molecular loss of function by aggregation translates to gain of toxic phenotype.

Discussion

About 30 amyloidogenic proteins are known to contribute to human disease. These diseases include neurodegenerative diseases such as Alzheimer's or Parkinson's disease but also organ-specific and systemic amyloidosis such as diabetes mellitus type 2 or light chain amyloidosis (*7*). Although the pathophysiological profiles of these diseases are disparate—involving the aggregation of different proteins, affecting distinctive cell types or tissues, and having very different progression rates—they also share common structural, biochemical, and biological features, suggesting that amyloids might also have similar modes of interaction with cellular components (*8*). Although amyloids of different proteins have been shown to interact with lipids (*40*), proteins (*41*), and nucleic acids (*42*), it is currently unclear which of these interactions are relevant for disease. Although some amyloid interactions are rather unspecific—for example, with biological lipids (*43*)—other amyloid interactions are highly specific (*20*). The most prominent of these is the self-interaction of amyloidogenic sequences during amyloid fibril formation, which includes both amyloid nucleation and fiber elongation (*44*, *45*). Proteome-wide studies using amyloid prediction algorithms suggest that most proteins possess amyloidogenic sequence segments within their structure, even though they do not form amyloid under normal conditions (*5*, *6*). Given the sequence specificity of amyloid seeding, this suggests that amyloid aggregation should be specifically inducible in non–amyloid-associated proteins by exposing them to amyloidogenic peptides derived from their own sequence.

Here, we demonstrate that aggregation of endogenously expressed VEGFR2 can be induced under physiological conditions by exposing it to vascin, a peptide consisting of a tandem repeat of an amyloidogenic sequence in its signal peptide. We found that vascin possesses all attributes of natural amyloids, including cross-β structure, the population of amyloid precursor aggregates, and the ability to reach the cytoplasmic compartment of cells, confirming that the signal peptide of VEGFR2 possesses a genuine amyloidogenic sequence. In addition, we found that vascin is able to induce VEGFR2 aggregation through direct interaction with VEGFR2. Because vascin is targeting the VEGFR2-signaling peptide, seeding of VEGFR2 aggregation is likely to be cotranslational, as suggested by ribosomal colocalization of vascin in the cytoplasm and the occurrence of partial VEGFR2 degradation along with its aggregation. This results in VEGFR2 inactivation in vitro but also in vivo, where it inhibits VEGFR2-dependent tumor growth upon intravascular administration. Both the aggregation as well as the inhibition of VEGFR2 appear to be specific. Scrambled vascin or the proline mutant do not interact with VEGFR2, nor does it provoke VEGFR2 aggregation or inhibition. In addition, whereas vascin suppresses cell-surface presentation of VEGFR2, it does not affect trafficking of other receptors such as CD29 or EGFR. Last, vascin-induced VEGFR2 aggregation is not inherently toxic because it does not affect the viability of VEGFR2-overexpressing HEK293 cells. Together, these findings show that VEGFR2, a protein not associated with amyloid disease, can be specifically induced to aggregate in the presence of specific amyloid seeds that are derived from its own sequence.

There may be multiple reasons why large-scale amyloidosis is not observed under natural conditions despite the likely prevalence of potentially amyloidogenic sequences in many proteins. First, most amyloidogenic sequences are buried in globular protein domains, which is probably the main protective factor against amyloidosis (*46*). Moreover, most misfolded proteins will be actively degraded in the cell before they have the opportunity to aggregate (*47*). Second, even in unfolded or intrinsically disordered proteins, most amyloidogenic sequences are generally still sufficiently protected from aggregation by structural mechanisms such as gatekeeping (the inhibition of aggregation by charged residues adjacent to the amyloidogenic segment) (*48*) and entropic bristles (unstructured protein segments that entropically prevent the association of amyloidogenic sequences) (*49*). Last, interaction with molecular chaperones will also contribute to the inhibition of aggregation (*50*). The reason why vascin can overcome these potential protective mechanisms is not yet clear but might reside in its design; vascin comprises a tandem repeat of an amyloidogenic sequence, which exacerbates the aggregation propensity of this sequence and leads to the formation of soluble and stable oligomeric aggregates, and these are likely to provide efficient sites for seeding. Incidentally, yeast prions often consist of peptide sequence repeats (*32*), and the stability of soluble oligomers consisting of tandem peptide repeats recently allowed their structure solvation by means of x-ray crystallography (*29*).

The toxic gain of function observed in many amyloid-associated diseases remains poorly explained. This is mainly due to the impossibility of relating loss-of-function effects to the aggregation process of a given protein. For many amyloid proteins, especially in neurodegeneration, the functional role of the affected protein is often complex and not entirely understood (*25*, *26*), which makes it difficult to unequivocally identify loss-of-function effects. In addition, the interactions of amyloid with cellular components in disease are also not clarified, so that again gain of toxic function is not directly tractable at the molecular level. The availability of our artificial amyloid model provides an opportunity to study the relationship between amyloid toxicity and specific protein loss of function. While recapitulating essential amyloid features, our model also allows monitoring the effect of amyloidosis on a functionally well-characterized protein. Moreover, the use of a VEGFR2 fragment allows the assessment of amyloid toxicity independent of VEGFR2 function.

Our results demonstrate that using this setup, vascin does not display generic toxic properties but rather the contrary. Vascin gain of function is specific (it is dependent on the presence of VEGFR2) but also conditional (VEGFR2 needs to be expressed in the cell, but the cell also needs to be dependent on VEGFR2 for its survival and proliferation). In VEGFR2-dependent HUVECs, vascin toxicity and VEGFR2 loss of function correlate in a dose-responsive manner, whereas this is not the case in VEGFR2-expressing HEK293 cells. Therefore, together these results illustrate how amyloid toxicity can result from a conjunction of protein-specific and cell-dependent protein loss of function. Whether lack of generalized toxicity is coupled to the availability of specific "aggregation epitopes" during or after translation remains to be further explored. It is possible that only selected APRs, occurring in the right structural context, would be sensitive to co-aggregation. However, the results in other model systems, such as plants (*31*) and bacteria (*30*), suggest that this is not the most likely scenario, but that the selectivity comes from the seqeunce specificity of the amyloid interaction (*20*, *51*). Further studies are needed to clarify this point.

Materials and methods

Bioinformatics

We used the TANGO algorithm for all APR identifications in this manuscript. We used a cutoff on the TANGO score of 5 per residue since this gives a Mathews Correlation Coefficient between prediction and experiment of 0.92 (*28*). The settings of TANGO were Temperature = 298 K, pH = 7.5, Ionic Strength = 0.10 M.

Peptides

Peptides were synthesized in-house using an Intavis Multipep RSi synthesis robot. Raw peptides were stored as dry ether precipitates at −20°C prior to use. Purified peptides were lyophilized and closed under nitrogen atmosphere and stored at −20°C prior to use. Stock solutions of each peptide were prepared fresh in 1% w/v ammonium bicarbonate in MiliQ water, filtered through 0.22 μm regenerated cellulose filter (Whatman, USA) and used immediately. The concentration of the peptides stocks was determined by absorbance at 280 nm using the calculated molar extinction coefficient $\varepsilon = 11380\ M^{-1}cm^{-1}$.

Cell lines and media

HUVEC cells (Lonza) were grown in EGM2 complete medium (Lonza) in flasks pre-coated with 0.1% gelatin. The cells were never allowed to grow confluent and were only used for experiments between passage p3 and p9. U2-Os and HEK293 cells were maintained in DMEM medium, supplemented with 10% FBS, 1 mM sodium pyruvate, non-essential amino acids and antibiotics (penicillin/streptomycin). Lipofectamine 2000 (Life Technologies) was used to transiently transfect HEK293 and U2OS cells with an expression vector for VEGFR2 (pCDNA3) generating the cell lines $HEK293^{VEGFR2}$ and $U2OS^{VEGFR2}$. All peptide treatments were done in DMEM/F12 medium without additives. Toxicity of the peptide treatments was evaluated using the CellTiter-Blue Cell Viability Assay according to the instructions of the manufacturer (Promega, USA).

Quantification of growth factor signaling

HUVEC, HEK293, U2OS, $HEK293^{VEGFR2}$ and $U2OS^{VEGFR2}$ cells were treated with peptide overnight. The next day cells were stimulated with 25 ng/ml recombinant mouse-VEGF (493-MV, R&D Systems) or recombinant human-EGF (236-EG, R&D Systems) for exactly 5 min at 37°C. Cells were washed twice with ice cold PBS and lysed in RIPA lysis buffer (ThermoFisher Scientific) supplement with Complete protease inhibitor (Roche) and PhosSTOP phosphatase inhibitor (Roche). Quantification of VEGFR2 autophosphorylation and ERK phosphorylation was performed by electrochemiluminescence ELISA using the following kits according to the manufacturer's recommended protocol: Phospho-VEGFR-2(Tyr1054) (K151DJD, Meso Scale Discovery) and Phospho(Thr202/Tyr204; Thr185/Tyr187)/Total ERK1/2 (K15107D, Meso Scale Discovery).

X-ray fiber diffraction

X-ray fiber diffraction samples were made by allowing a droplet of the stock fibril solution to dry between two wax tipped capillary tubes. X-ray diffraction data was collected using a Rigaku rotating anode (CuKa) with Saturn CCD detector with exposure times of 30–60 s and specimen to detector distance of 50 or 100 mm. Reflections were measured using CLEARER (*52*).

In vivo experiments

All animal procedures were approved by the local animal ethical committee. Female C57BL/6 mice, 8 weeks of age, were purchased from Janvier (France). The B16.F10 melanoma cell line was obtained from the American Type Culture Collection (ATCC) and maintained in Dulbecco's Modified Eagle's Medium (DMEM) supplemented with 10% fetal bovine serum. B16 cells (5×10^5 cells/mouse) were implanted subcutaneously in the right dorsal flank of C57BL/6 mice. Starting from 3 days after tumor implantation, mice were randomized in three groups and treated daily by intravenous delivery of vascin or scrambled vascin (10mg/kg), or by oral delivery of PTK787 (75mg/kg). Tumors growth was monitored by caliper measurement every 2–3 days starting from 10 days after tumor injection. The experiment had 10 animals per group at onset, except the PTK group, which had five.

Transmission Electron Microscopy (TEM)

For each sample 7 μL aliquots of peptide solution were adsorbed for 1 min to formvar film coated copper grids of 400-mesh (Agar Scientific Ltd., England) that were first glow discharged to improve adsorption. After sample adsorption grids were washed by contact with 5 drops of ultrapure water and stained by contact with one drop of uranyl acetate (2% w/v in MiliQ water) for 45 s. The grids were examined using a JEM-2100 transmission electron microscope (Jeol, Japan) at 80 keV.

Biophysical characterization

Dynamic light scattering (DLS) measurements were made at room temperature with a DynaPro DLS plate reader instrument (Wyatt, Santa Barbara, CA, USA) equipped with a 830-nm laser source. Samples (100 μL 300 μM peptide stock) were placed into a flat-bottom 96-well microclear plate (Greiner, Germany). The autocorrelation of scattered light intensity at a 90° angle was recorded for 10 s and averaged over 40 recordings to obtain a single data point. The Wyatt Dynamics software was used to calculate the hydrodynamic radius by assuming linear polymer particles. Attenuated Total Reflection Fourier Transform Infrared Spectroscopy (ATR FTIR) was performed using a Bruker Tensor 27 infrared spectrophotometer (Bruker, Germany) equipped with a Bio-ATR II accessory (Harrick Scientific Products, USA). Spectra were recorded in the range of 900–3500 cm^{-1} at a spectral resolution of 2 cm^{-1} by accumulating 256 data acquisitions. The spectrophotometer was continuously purged with dried air. Spectra were corrected for atmospheric water vapor interference, baseline-subtracted, and vector normalized in the amide II area (1500 to 1600 cm-1) as implemented in OPUS software (Bruker). Tinctorial analysis was performed by incubating vascin or its scrambled version at the concentration indicated on each figure with 20 μM ThT, 20 μM ANS or 0.3 μM h-HTAA and fluorescence emission was recorded in a PolarStar Optima plate reader (BMG labtech, Germany) equipped with 360 nm and 490 nm excitation filters and 460 nm and 520 nm emission filters. All filters had 10 nm band-pass. Emission fluorescence spectra of h-HTAA bound to vascin or scrambled vascin were recorded in a FlexStation 3 (Molecular Devices, USA) at the same concentration of peptide and fluorophore listed above, with excitation at 480 nm and emission recorded between 490 nm and 620 nm using 10 nm band-pass.

Statistics

Statistical analysis was performed using Prism, Origin or R. Unpaired student's *t* test and ANOVA

were used to determine significant differences between samples unless otherwise indicated. Significance levels: * for $P < 0.05$, ** for $P < 0.01$, *** for $P < 0.001$.

REFERENCES AND NOTES

1. K. Dudgeon, K. Famm, D. Christ, Sequence determinants of protein aggregation in human VH domains. *Protein Eng. Des. Sel.* **22**, 217–220 (2009). doi: 10.1093/protein/gzn059; pmid: 18957405
2. S. Ventura *et al.*, Short amino acid stretches can mediate amyloid formation in globular proteins: The Src homology 3 (SH3) case. *Proc. Natl. Acad. Sci. U.S.A.* **101**, 7258–7263 (2004). doi: 10.1073/pnas.0308249101; pmid: 15123800
3. O. S. Makin, L. C. Serpell, Structures for amyloid fibrils. *FEBS J.* **272**, 5950–5961 (2005). doi: 10.1111/j.1742-4658.2005.05025.x; pmid: 16302960
4. D. Eisenberg *et al.*, Amyloid and prion structures. *FASEB J.* **23**, 423 (2009).
5. F. Rousseau, L. Serrano, J. W. H. Schymkowitz, How evolutionary pressure against protein aggregation shaped chaperone specificity. *J. Mol. Biol.* **355**, 1037–1047 (2006). doi: 10.1016/j.jmb.2005.11.035; pmid: 16359707
6. L. Goldschmidt, P. K. Teng, R. Riek, D. Eisenberg, Identifying the amylome, proteins capable of forming amyloid-like fibrils. *Proc. Natl. Acad. Sci. U.S.A.* **107**, 3487–3492 (2010). doi: 10.1073/pnas.0915166107; pmid: 20133726
7. F. Chiti, C. M. Dobson, Protein misfolding, functional amyloid, and human disease. *Annu. Rev. Biochem.* **75**, 333–366 (2006). doi: 10.1146/annurev.biochem.75.101304.123901; pmid: 16756495
8. D. Eisenberg, M. Jucker, The amyloid state of proteins in human diseases. *Cell* **148**, 1188–1203 (2012). doi: 10.1016/j.cell.2012.02.022; pmid: 22424229
9. K. E. Marshall, R. Marchante, W. F. Xue, L. C. Serpell, The relationship between amyloid structure and cytotoxicity. *Prion* **8**, 192–196 (2014). doi: 10.4161/pri.28860; pmid: 24819071
10. M. R. Krebs *et al.*, Formation and seeding of amyloid fibrils from wild-type hen lysozyme and a peptide fragment from the beta-domain. *J. Mol. Biol.* **300**, 541–549 (2000). doi: 10.1006/jmbi.2000.3862; pmid: 10884350
11. J. T. Jarrett, E. P. Berger, P. T. Lansbury Jr., The carboxy terminus of the beta amyloid protein is critical for the seeding of amyloid formation: Implications for the pathogenesis of Alzheimer's disease. *Biochemistry* **32**, 4693–4697 (1993). doi: 10.1021/bi00069a001; pmid: 8490014
12. W. Li *et al.*, Aggregation promoting C-terminal truncation of alpha-synuclein is a normal cellular process and is enhanced by the familial Parkinson's disease-linked mutations. *Proc. Natl. Acad. Sci. U.S.A.* **102**, 2162–2167 (2005). doi: 10.1073/pnas.0406976102; pmid: 15684072
13. Y. Wang, S. Garg, E. M. Mandelkow, E. Mandelkow, Proteolytic processing of tau. *Biochem. Soc. Trans.* **38**, 955–961 (2010). doi: 10.1042/BST0380955; pmid: 20658984
14. S. Nyström, P. Hammarström, Generic amyloidogenicity of mammalian prion proteins from species susceptible and resistant to prions. *Sci Rep* **5**, 10101 (2015). doi: 10.1038/srep10101; pmid: 25960067
15. R. S. Rajan, M. E. Illing, N. F. Bence, R. R. Kopito, Specificity in intracellular protein aggregation and inclusion body formation. *Proc. Natl. Acad. Sci. U.S.A.* **98**, 13060–13065 (2001). doi: 10.1073/pnas.181479798; pmid: 11687604
16. M. R. Krebs, L. A. Morozova-Roche, K. Daniel, C. V. Robinson, C. M. Dobson, Observation of sequence specificity in the seeding of protein amyloid fibrils. *Protein Sci.* **13**, 1933–1938 (2004). doi: 10.1110/ps.04707004; pmid: 15215533
17. J. Xu *et al.*, Gain of function of mutant p53 by coaggregation with multiple tumor suppressors. *Nat. Chem. Biol.* **7**, 285–295 (2011). doi: 10.1038/nchembio.546; pmid: 21445056
18. K. Ono, R. Takahashi, T. Ikeda, M. Yamada, Cross-seeding effects of amyloid β-protein and α-synuclein. *J. Neurochem.* **122**, 883–890 (2012). doi: 10.1111/j.1471-4159.2012.07847.x; pmid: 22734715
19. M. E. Oskarsson *et al.*, In vivo seeding and cross-seeding of localized amyloidosis: A molecular link between type 2 diabetes and Alzheimer disease. *Am. J. Pathol.* **185**, 834–846 (2015). doi: 10.1016/j.ajpath.2014.11.016; pmid: 25700985
20. A. Ganesan *et al.*, Selectivity of aggregation-determining interactions. *J. Mol. Biol.* **427**, 236–247 (2015). doi: 10.1016/j.jmb.2014.09.027; pmid: 25451783
21. W. Surmacz-Chwedoruk, V. Babenko, W. Dzwolak, Master and slave relationship between two types of self-propagating insulin amyloid fibrils. *J. Phys. Chem. B* **118**, 13582–13589 (2014). doi: 10.1021/jp510980b; pmid: 25373010
22. K. H. Ashe, A. Aguzzi, Prions, prionoids and pathogenic proteins in Alzheimer disease. *Prion* **7**, 55–59 (2013). doi: 10.4161/pri.23061; pmid: 23208281
23. K. F. Winklhofer, J. Tatzelt, C. Haass, The two faces of protein misfolding: Gain- and loss-of-function in neurodegenerative diseases. *EMBO J.* **27**, 336–349 (2008). doi: 10.1038/sj.emboj.7601930; pmid: 18216876
24. M. Jucker, L. C. Walker, Self-propagation of pathogenic protein aggregates in neurodegenerative diseases. *Nature* **501**, 45–51 (2013). doi: 10.1038/nature12481; pmid: 24005412
25. H. A. Pearson, C. Peers, Physiological roles for amyloid beta peptides. *J. Physiol.* **575**, 5–10 (2006). doi: 10.1113/jphysiol.2006.111203; pmid: 16809372
26. J. T. Bendor, T. P. Logan, R. H. Edwards, The function of α-synuclein. *Neuron* **79**, 1044–1066 (2013). doi: 10.1016/j.neuron.2013.09.004; pmid: 24050397
27. I. Benilova, E. Karran, B. De Strooper, The toxic Aβ oligomer and Alzheimer's disease: An emperor in need of clothes. *Nat. Neurosci.* **15**, 349–357 (2012). doi: 10.1038/nn.3028; pmid: 22286176
28. A. M. Fernandez-Escamilla, F. Rousseau, J. Schymkowitz, L. Serrano, Prediction of sequence-dependent and mutational effects on the aggregation of peptides and proteins. *Nat. Biotechnol.* **22**, 1302–1306 (2004). doi: 10.1038/nbt1012; pmid: 15361882
29. A. Laganowsky *et al.*, Atomic view of a toxic amyloid small oligomer. *Science* **335**, 1228–1231 (2012). doi: 10.1126/science.1213151; pmid: 22403391
30. N. G. Bednarska *et al.*, Protein aggregation as an antibiotic design strategy. *Mol. Microbiol.* **99**, 849–865 (2016). doi: 10.1111/mmi.13269; pmid: 26559925
31. C. Betti *et al.*, Sequence-specific protein aggregation generates defined protein knockdowns in plants. *Plant Physiol.* **171**, 773–787 (2016). pmid: 27208282
32. E. D. Ross, A. Minton, R. B. Wickner, Prion domains: Sequences, structures and interactions. *Nat. Cell Biol.* **7**, 1039–1044 (2005). doi: 10.1038/ncb1105-1039; pmid: 16385730
33. R. Sabate, F. Rousseau, J. Schymkowitz, S. Ventura, What makes a protein sequence a prion? *PLOS Comput. Biol.* **11**, e1004013 (2015). doi: 10.1371/journal.pcbi.1004013; pmid: 25569335
34. T. Klingstedt *et al.*, Synthesis of a library of oligothiophenes and their utilization as fluorescent ligands for spectral assignment of protein aggregates. *Org. Biomol. Chem.* **9**, 8356–8370 (2011). doi: 10.1039/c1ob05637a; pmid: 22051883
35. L. M. Young *et al.*, Screening and classifying small-molecule inhibitors of amyloid formation using ion mobility spectrometry-mass spectrometry. *Nat. Chem.* **7**, 73–81 (2015). doi: 10.1038/nchem.2129; pmid: 25515893
36. S. Campioni *et al.*, A causative link between the structure of aberrant protein oligomers and their toxicity. *Nat. Chem. Biol.* **6**, 140–147 (2010). doi: 10.1038/nchembio.283; pmid: 20081829
37. D. Pinotsi *et al.*, Direct observation of heterogeneous amyloid fibril growth kinetics via two-color super-resolution microscopy. *Nano Lett.* **14**, 339–345 (2014). doi: 10.1021/nl4041093; pmid: 24303845
38. J. M. Wood *et al.*, PTK787/ZK 222584, a novel and potent inhibitor of vascular endothelial growth factor receptor tyrosine kinases, impairs vascular endothelial growth factor-induced responses and tumor growth after oral administration. *Cancer Res.* **60**, 2178–2189 (2000). pmid: 10786682
39. R. Radde *et al.*, Aβ42-driven cerebral amyloidosis in transgenic mice reveals early and robust pathology. *EMBO Rep.* **7**, 940–946 (2006). doi: 10.1038/sj.embor.7400784; pmid: 16906128
40. H. A. Lashuel, D. Hartley, B. M. Petre, T. Walz, P. T. Lansbury Jr., Neurodegenerative disease: Amyloid pores from pathogenic mutations. *Nature* **418**, 291 (2002). doi: 10.1038/418291a; pmid: 12124613
41. H. Olzscha *et al.*, Amyloid-like aggregates sequester numerous metastable proteins with essential cellular functions. *Cell* **144**, 67–78 (2011). doi: 10.1016/j.cell.2010.11.050; pmid: 21215370
42. D. Cirillo *et al.*, Neurodegenerative diseases: Quantitative predictions of protein-RNA interactions. *RNA* **19**, 129–140 (2013). doi: 10.1261/rna.034777.112; pmid: 23264567
43. G. P. Gorbenko, P. K. Kinnunen, The role of lipid-protein interactions in amyloid-type protein fibril formation. *Chem. Phys. Lipids* **141**, 72–82 (2006). doi: 10.1016/j.chemphyslip.2006.02.006; pmid: 16569401
44. R. Wetzel, Kinetics and thermodynamics of amyloid fibril assembly. *Acc. Chem. Res.* **39**, 671–679 (2006). doi: 10.1021/ar050069h; pmid: 16981684
45. S. I. Cohen *et al.*, Proliferation of amyloid-β42 aggregates occurs through a secondary nucleation mechanism. *Proc. Natl. Acad. Sci. U.S.A.* **110**, 9758–9763 (2013). doi: 10.1073/pnas.1218402110; pmid: 23703910
46. F. Chiti, C. M. Dobson, Amyloid formation by globular proteins under native conditions. *Nat. Chem. Biol.* **5**, 15–22 (2009). doi: 10.1038/nchembio.131; pmid: 19088715
47. G. De Baets *et al.*, An evolutionary trade-off between protein turnover rate and protein aggregation favors a higher aggregation propensity in fast degrading proteins. *PLOS Comput. Biol.* **7**, e1002090 (2011). pmid: 21731483
48. G. De Baets, J. Van Durme, F. Rousseau, J. Schymkowitz, A genome-wide sequence-structure analysis suggests aggregation gatekeepers constitute an evolutionary constrained functional class. *J. Mol. Biol.* **426**, 2405–2412 (2014). doi: 10.1016/j.jmb.2014.04.007; pmid: 24735868
49. A. A. Santner *et al.*, Sweeping away protein aggregation with entropic bristles: Intrinsically disordered protein fusions enhance soluble expression. *Biochemistry* **51**, 7250–7262 (2012). doi: 10.1021/bi300653m; pmid: 22924672
50. R. I. Morimoto, The heat shock response: Systems biology of proteotoxic stress in aging and disease. *Cold Spring Harb. Symp. Quant. Biol.* **76**, 91–99 (2011). doi: 10.1101/sqb.2012.76.010637; pmid: 22371371
51. J. R. Couceiro *et al.*, Sequence-dependent internalization of aggregating peptides. *J. Biol. Chem.* **290**, 242–258 (2015). doi: 10.1074/jbc.M114.586636; pmid: 25391649
52. S. Zibaee, O. S. Makin, M. Goedert, L. C. Serpell, A simple algorithm locates beta-strands in the amyloid fibril core of alpha-synuclein, Aβ, and τ using the amino acid sequence alone. *Protein Sci.* **16**, 906–918 (2007).

ACKNOWLEDGMENTS

This work was supported by the European Research Council (ERC) under the European Union's Horizon 2020 Framework Programme, ERC grant agreement 647458 (MANGO) to J.S. The Switch Laboratory was supported by grants from VIB, Industrial Research Funds of KU Leuven (IOF), the Funds for Scientific Research Flanders (FWO), the Flanders Institute for Science and Technology (IWT), and the Federal Office for Scientific Affairs of Belgium (Belspo), IUAP P7/16. G.V.V., F.D.S., and F.C. were supported by postdoctoral fellowships of FWO. G.V.V. was also supported by KU Leuven competitive funding (PF/10/014). L.Y. is funded by a Wellcome Trust Institutional Strategic Support Fund (ISSF) (grant 015615/Z/14/Z). The Synapt high-definition mass spectroscopy mass spectrometer was purchased with funds from the Biotechnology and Biological Sciences Research Council through its Research Equipment Initiative scheme (BB/E012558/1). The Linköping University laboratories were supported by The Göran Gustafsson Foundation, The Swedish Research Council, and The Swedish Alzheimer Foundation. P.C. was supported by FWO, Methusalem funding by the Flemish government, and an AXA Research grant. M.K. is supported by a Marie Skłodowska-Curie Individual Fellowship under the European Union's Horizon 2020 Framework Programme (grant H2020-MSCA-IF-2014-ST). C.V. was supported by the KU Leuven Stem Cell Programme. F.R. and J.S. are inventors on patent applications WO2007/071789 and WO2012/123419 submitted by VIB vzw, Belgium, that covers the use of targeted protein aggregation for therapeutic or biotechnological applications. The authors declare no other financial interests in this work. B.D.S. also held an appointment with the Institute of Neurology, University College of London, UK, and is a paid consultant for Janssen Pharmaceuticals NV, Belgium, and Remynd NV, Belgium. Human embryonic stem H9 cells are available from the University of Wisconsin under a materials transfer agreement.

SUPPLEMENTARY MATERIALS

www.sciencemag.org/content/354/6313/aah4949/suppl/DC1
Materials and Methods
Supplementary Text
Figs. S1 to S15
Tables S1 to S3
References (*53*–*67*)

6 July 2016; accepted 23 September 2016
10.1126/science.aah4949

Science
AAAS

De novo design of a biologically active amyloid

Rodrigo Gallardo, Meine Ramakers, Frederik De Smet, Filip Claes, Ladan Khodaparast, Laleh Khodaparast, José R. Couceiro, Tobias Langenberg, Maxime Siemons, Sofie Nyström, Laurence J. Young, Romain F. Laine, Lydia Young, Enrico Radaelli, Iryna Benilova, Manoj Kumar, An Staes, Matyas Desager, Manu Beerens, Petra Vandervoort, Aernout Luttun, Kris Gevaert, Guy Bormans, Mieke Dewerchin, Johan Van Eldere, Peter Carmeliet, Greetje Vande Velde, Catherine Verfaillie, Clemens F. Kaminski, Bart De Strooper, Per Hammarström, K. Peter R. Nilsson, Louise Serpell, Joost Schymkowitz and Frederic Rousseau (November 10, 2016)
Science **354** (6313), . [doi: 10.1126/science.aah4949]

Editor's Summary

Aggregation by design

Amyloid aggregation is driven by short sequences within proteins that self-assemble into characteristic amyloid structures. About 30 human proteins are implicated in amyloid-associated diseases, but many more contain short sequences that are potentially amyloidogenic. Gallardo *et al.* designed a peptide based on an amyloidogenic sequence in the vascular endothelial growth factor receptor VEGFR2. The peptide induced VEGFR2 to form aggregates with features characteristic of amyloids. Amyloids were toxic only in cells that required VEGFR2 activity, suggesting that the toxicity was due to loss of function of VEGFR2, rather than to inherent toxicity of the aggregates. The peptide inhibited VEGFR2-dependent tumor growth in a mouse tumor model.

Science, this issue p. 10.1126/science.aah4949